JOURNAL OF ADVANCED TRANSPORTATION
J. Adv. Transp. 2014; **48**:165–184
Published online 13 September 2013 in Wiley Online Library (wileyonlinelibrary.com). DOI: 10.1002/atr.1248

A new kind of fundamental diagram with an application to road traffic emission modeling

Vincent Aguiléra* and Antoine Tordeux

Laboratoire Ville Mobilité Transport, Université Paris-Est, Ecole des Ponts ParisTech, 6&8 Avenue Blaise Pascal, Cité Descartes, Champs sur Marne F-77455 Marne-la-Vallée, France

SUMMARY

The main contribution of this paper is to show, on the basis of empirical traffic data, that the distribution of vehicle speeds on a road segment evolves with the occupancy in a simple manner. Under a critical occupancy, the distribution is unimodal, with one peak (the high mode) close to the free-flow speed. When the occupancy exceeds the critical occupancy, the distribution of speeds becomes bimodal. A second peak (the low mode) appears, at a noticeably lower speed than the high mode. Empirical speed distributions are well fitted when assuming a (appropriately scaled and translated) low "temperature" Maxwell–Boltzmann distribution for the high mode and a high-temperature distribution for the low mode. The standard fundamental diagram expresses the mean flow speed as a function of occupancy. The model proposed in this paper expresses the distribution of vehicle speeds as a function of the occupancy. We believe this result to be of great importance for both the theory of traffic flow and practical applications. Copyright © 2013 John Wiley & Sons, Ltd.

KEY WORDS: highway and traffic engineering; density; flow; speed

1. INTRODUCTION

The new generation of road traffic emission models is modal-based. They rely on a fine grain description of the various modes a fleet of vehicles is operated on a network, an operating mode being essentially characterized by a driving cycle. Preparing the necessary traffic activity data is a huge challenge. Precise measurements of vehicle operation and location are expensive to collect. At the same time, most road networks are equipped with traffic flow sensors. Point-based measurements of macroscopic quantities (volume, occupancy, and speed) are available. But, to the authors' knowledge, no method has been proposed in the literature to disaggregate macroscopic flow variables into statistical distributions of vehicle operating modes. By contrast, the kinetic theory of gases tells that, in a volume of ideal gas at thermal equilibrium, the space average distribution of particles' speeds follows the Maxwell–Boltzmann distribution. The system is ergodic: the time average distribution of speed along particles' trajectories equates the space average distribution of speeds. Hence, a single point-based measurement of a macroscopic quantity, the temperature, is needed to estimate the distribution of particles' speeds along their trajectories.

The main contribution of this paper is to show, on the basis of empirical 30-second traffic data, that similar conclusions seem to be drawn for traffic flows. The distribution of vehicle speeds on a road segment evolves with the occupancy in a simple manner. Under a critical occupancy, the distribution is unimodal, with one peak (the high mode) close to the free-flow speed. When the occupancy exceeds the critical occupancy, the distribution of speeds becomes bimodal. A second peak (the low mode)

*Correspondence to: Vincent Aguiléra, Laboratoire Ville Mobilité Transport, Université Paris-Est, Ecole des Ponts ParisTech, 6&8 Avenue Blaise Pascal, Cité Descartes, Champs sur Marne, F-77455 Marne-la-Vallée, France. E-mail: vincent.aguilera@enpc.fr

appears, at a noticeably lower speed than the high mode. Empirical speed distributions are well fitted when assuming a (appropriately scaled and translated) low "temperature" Maxwell–Boltzmann distribution for the high mode and a high-temperature distribution for the low mode. We believe this intriguing result to be of great importance for both the theory of traffic flow and practical applications.

This paper concentrates on the latter and is organized as follows. Empirical traffic data are analyzed at various time scales in Section 2. It provides the necessary inputs to Section 3, where the distributions of vehicle speeds in congested traffic are shown to be well fitted, for various occupancy values, by a simple bimodal model. Section 4 presents an application to fuel consumption (FC) estimates. The conclusion follows.

2. EMPIRICAL DATA ANALYSIS

This section provides the necessary inputs to the other parts of the paper. It studies the distribution of empirical traffic flow data at various time scales. The dataset contains 30-second occupancy-volume-speed records from paired loop detectors, collected during 10 consecutive days. More details are given in Section 2.1. When averaged over the study period (Section 2.2), simple relations appear between the flow macroscopic variables. Peak periods are well identified. Then in Section 2.3, the hourly variations of the distribution of 6-minute average speed are studied, with a particular attention paid to the evening peak hour. No typical hourly distribution of 6-minute average speeds can be observed. This will be of importance in Section 4, because some emission models do rely on this assumption to model traffic activity data. Finally in Section 2.4 the dispersion of 30-second data (speed and occupancy) is studied, during the study period as a whole, and also within 6-minute intervals. It is shown that although 30-second occupancy values are asymmetrically scattered within 6-minute intervals, 30-second speed values appear normally distributed with a small variance. This observation support the assumptions made in Section 3 to estimate the distribution of vehicle speeds from flow data.

2.1. The I-80 dataset

The data used in this section, and referenced hereafter as the *I-80 dataset*, have been collected during the Next Generation SIMulation (NGSIM) program on eastbound I-80 in Emeryville, San Francisco Bay Area, California. They are freely available at the NGSIM website.[1] The study area was approximately 500 meters in length. It comprised six lanes. The left-most lane, numbered 1, is a high-occupancy vehicle (HOV) lane. Lane 6 is a merge/exit lane. The study area was equipped with eight equally spaced paired loop detectors stations. Each station had one detector per lane. The data covers a period of 10 consecutive days, starting from Thursday, April 7, with a record every 30 seconds, for a total amount of 28 800 records per lane and per station. Given a lane and a station, a record contains the 30-second mean occupancy, the 30-second vehicle count, and the 30-second mean flow speed.

2.2. Mean day

When averaged over the 10 days of the study period, and projected on the occupancy-speed plane and on the occupancy-flow plane, the mean values of 30-second data exhibit a well-known behavior (Figure 1a). Following the seminal works of Greenshield, traffic engineers assume the existence of a fundamental relation [1] between the mean speed (or mean flow) and the mean density (or occupancy[2]). When averaging empirical traffic data, a smooth concave curve emerges in the density-flow plane. The so-called *fundamental diagram* is the basis of hydrodynamic traffic models, where the flow mean speed, the flow mean density, and the mean flow rate are continuous scalar variables. From the fundamental diagram, traffic states are usually classified into two categories: free and congested. Free traffic states are observed when the density is lower than a threshold called the critical density. The

[1] http://www.ngsim-community.org

[2] Strictly speaking, the density is the concentration of vehicles over space, whereas the occupancy is the concentration of vehicles over time. For a point-based detector, density and occupancy are constant multiples of each other under the assumption of constant vehicle lengths.

DOI: 10.1002/atr

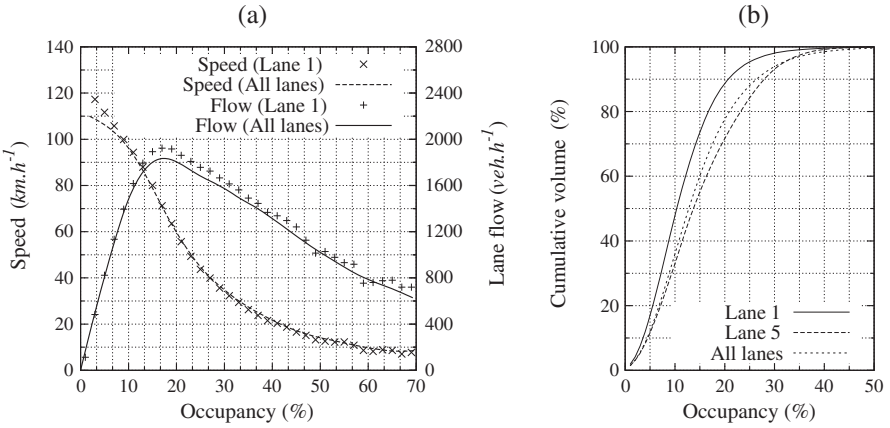

Figure 1. (a) Variations of the 10-day average speed and flow, for lanes 1 to 5, as a function of occupancy. (b) Normalized cumulative distribution of the volume during the study period, as a function of occupancy.

flow mean speed is high. The flow rate increases with the density. *A contrario*, congested traffic states are characterized by a density that exceeds the critical density. The flow rate and the flow speed decrease when the flow density increases. For the I-80 dataset, and for all lanes from 1 to 5, and according to the fundamental diagram, the critical occupancy is between 16% and 18%, and the maximum flow rate per lane is around $1,800 veh.h^{-1}$ (Figure 1a). The HOV lane (lane 1) has a fundamental diagram very similar to that of the average of the other lanes.

It will be shown later on that congestion effects appear when occupancy exceeds 10%, below the critical density identified from the fundamental diagram. The fraction of traffic volume observed when occupancy exceeds 10% (i.e., in congested driving conditions) can be drawn from Figure 1b, where the cumulative distribution of volume observed during the study period, as a function of occupancy, is plotted for lane 1, lane 5, and all lanes. On average, for all lanes, more than 60% of the total traffic volume was observed in congested driving conditions. This percentage varies with the lane. Lane 5 is above the average. Lane 1 is below the average, at around 50%.

2.3. Hourly variations of the distribution of 6-min average speed

The simple relations that appear in the fundamental diagram between the 10-day averages of the flow speed, the flow rate, and the occupancy do hide a more complex behavior when analyzed at smaller time scales. The speed profile (respectively, the occupancy profile) of the average day is plotted shown in Figure 2a (respectively, Figure 2b). The plots represent the 10-day average value of speed and occupancy, for all lanes from 1 to 5, for all stations, and for all 6-minute intervals during the day. The speed clearly decreases when the occupancy increases. In the early morning and in the late evening, the speed is close to the speed limit ($65 mph = 104 km.h^{-1}$). The morning and evening peaks are characterized by speed values below $80 km.h^{-1}$ and occupancy values above 15%. Between the morning and the evening peaks, the traffic remains congested. The speed remains below $90 km.h^{-1}$, and the occupancy above 10%. The grayed area around the speed curve (Figure 2a) illustrates how the 6-minute average speeds are dispersed around the 10-day average speed. It represents the interquartile range of the 6-minute speed values: 50% of the values are within the grayed area, 25% are above its upper boundary, and 25% are below its lower boundary. The interquartile range is narrow in free-flow conditions (i.e., when the occupancy is less than 10%). It widens when the occupancy exceeds 10%. The dispersion of occupancy follows a very similar pattern (Figure 2b).

From Figure 2a, the distribution of average speeds during the evening peak period, that is between 03:00 and 06:00 PM, appears quite stable. The 10-day average speed varies around $50 km.h^{-1}$. The bounds of the interquartile range, at $40 km.h^{-1}$ and $60 km.h^{-1}$, are symmetric. But this apparent regularity is misleading. In Figure 2c is plotted the range of variation of the 6-min average speed, as a function of the 1-hour average speed, for each 1-hour time slot included in the evening peak. The

DOI: 10.1002/atr

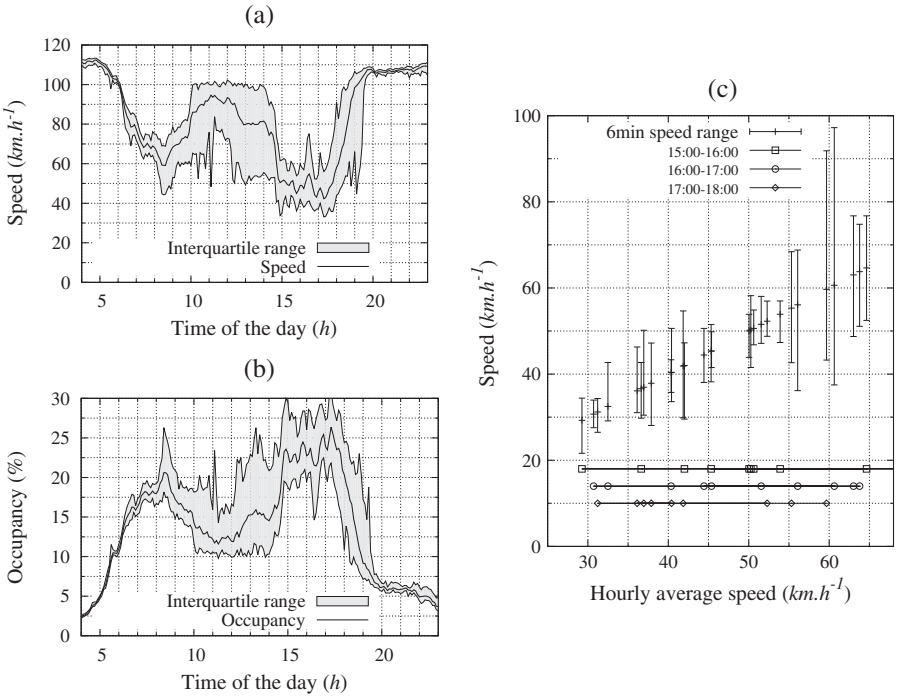

Figure 2. Variations of (a) speed and (b) occupancy during the average day of the study period, as a function of the time of the day. (c) Range of variation of 6-minute speed values, as a function of the hourly average speed in the evening peak period, between 03:00 and 06:00 PM.

1-hour average speed values are almost regularly dispersed between $30km.h^{-1}$ and $70km.h^{-1}$. The nine values[3] above $55km.h^{-1}$ correspond to the three-weekend days included in the study period (one Sunday and two Saturdays). The 21 others, between $30km.h^{-1}$ and $55km.h^{-1}$, correspond to weekdays. For weekdays, there is no apparent correlation between the 1-hour average speed and the range of variation of the 6-minute average speed, nor between the average speed and a particular hour within the evening peak period. If the latter was true, the symbols on the horizontal lines at the bottom of Figure 2c would be clustered together on each line. In short, for any two distinct weekdays, and for a given 1-hour time slot during the evening peak, the two distributions of 6-minute average speeds during this particular time slot are more likely to be disjoint than equal.

2.4. Dispersion of 30-second data

In the occupancy-speed plane, 6-minute average data are far less dispersed than 30-second data. Indeed, as illustrated at the top of Figure 3, 6-minute data are clustered around the fundamental diagram, whereas 30-second data are far more dispersed. This is true for all lanes, although only the plots for lane 1 (Figure 3a), lane 3 (Figure 3b), and lane 5 (Figure 3c) are shown here. If the dispersion of 30-second data was explained by a zero-mean Gaussian noise, one would expect a symmetric dispersion of the minimum and maximum 30-second values around the mean 6-minute values. This is not the case. At the bottom of Figure 3 are scatter plots of the minimum and maximum occupancy observed during all the 6-minute intervals of the study period, as a function of the 6-minute average occupancy, for lane 1 (Figure 3d), lane 3 (Figure 3e), and lane 5 (Figure 3f). Although not shown here, lanes 2 and 4 show very similar plots. Three comments can be made. First, the dispersion of 30-second occupancy values within all observed 6-minute intervals is quite high. All points are far from the diagonal. The few intervals during which the 30-second occupancy varies at a steady pace correspond

[3]Only seven appear on the plot; two are out of the plot's range.

DOI: 10.1002/atr

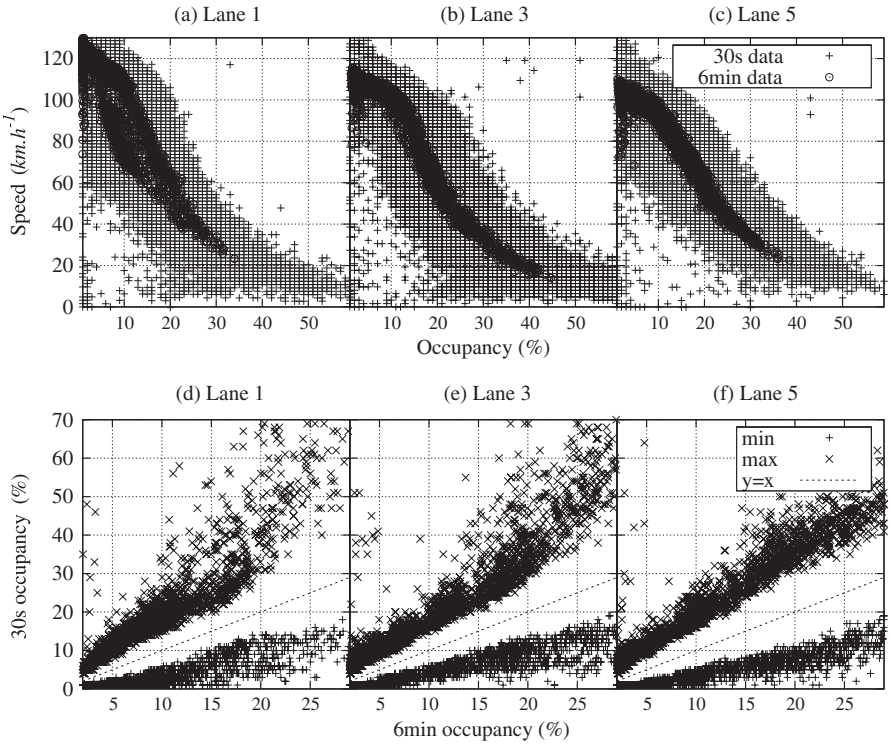

Figure 3. Top: dispersion of 30-second data and 6-minute average data, in the occupancy-speed plane. Bottom: scatter plot of the minimum and maximum occupancy observed during 6-minute intervals, as a function of the 6-minute average occupancy.

to very low 6-minute mean occupancy, below 5%. Second, this dispersion increases while the 6-minute average occupancy increases. The more congested the traffic, the more scattered is the 30-second occupancy within 6-minute intervals. Third, the dispersion of values around the average is not symmetric. For lane 3, and a 6-minute average occupancy between 20% and 25%, the minimum values vary between 5% and 10%, whereas the maximum values vary between 30% and 60%.

Figure 4a gives a better idea of the typical dispersion of 30-second occupancy values within 6-minute intervals. The plot represents the cumulative distribution of the *relative asymmetry index* (RAI) of occupancy values, the RAI being defined as follows. Let $X_i, i = 1 \ldots n$ denote the set of 30-second

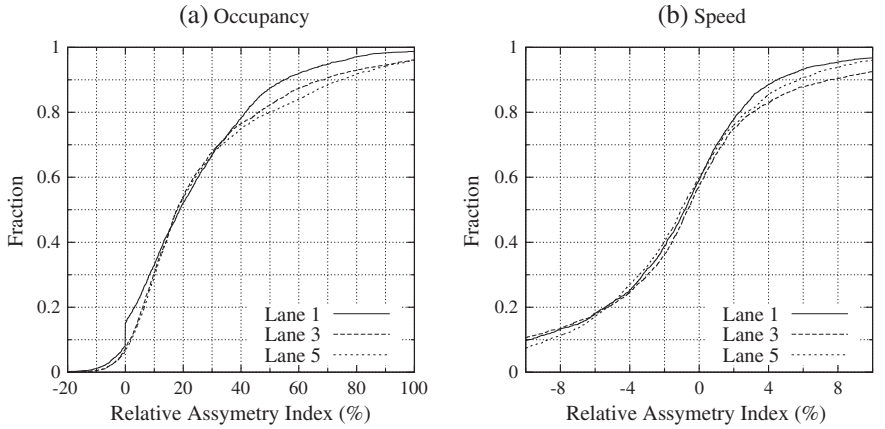

Figure 4. Dissymmetry index of 30-second data within 6-minute time slices. (a) Occupancy and (b) speed.

DOI: 10.1002/atr

measures contained in the i-th 6-minute interval during the study period, with $\overline{X}_i$ the mean value. RAI (X_i) is defined by

$$\mathrm{RAI}(X_i) = \frac{\frac{\max(X_i)+\min(X_i)}{2} - \overline{X}_i}{\overline{X}_i}$$

The RAI measures the distance between the midpoint of the minimum–maximum range, relatively to the mean point. If, on average, the 30-second values within each X_i are symmetrically distributed, then the distribution of RAI values during the study period can be expected to be zero-centered. As shown in (Figure 4a), the RAI distribution of occupancy is far from being zero-centered. For a mere half of the observed 6-minute intervals, the occupancy RAI is above 20%. Less than 10% of the 6-minute intervals have the midpoint of their minimum–maximum range within 10% of the 6-minute mean occupancy.

Interestingly, the RAI distribution of speeds follows a very different pattern (Figure 4b). The distribution is zero-centered, symmetric, with more than 60% values in the $[-5\% : +5\%]$ range and almost all values within the $[-10\% : +10\%]$ range. This suggests that 30-second flow speeds are normally distributed within 6-minute intervals, with a small standard deviation proportional to the 6-minute speed.

3. BIMODAL DISTRIBUTIONS OF VEHICULAR SPEEDS IN CONGESTED TRAFFIC

The bimodal nature of the distribution of vehicle speeds is not new to microscopic traffic modelers, at least for the cellular automata (CA) community. Indeed, the most simple traffic model one can possibly imagine is CA-184.[4] Vehicles are distributed on an infinite one-dimensional grid of cells, with at most one vehicle per cell. Vehicle speeds are taken in the set $\{0,1\}$. If the cell in front of a vehicle is empty, the vehicle jumps in it. If not, the vehicle stays in its cell. The fraction of vehicles having a zero speed increases when the occupancy increases. Similar patterns have been observed, although not modeled, for more sophisticated CA models [3]. This section starts by studying the distribution of vehicle speeds with a microscopic model (Section 3.1), when the free-flow speed and the mean occupancy vary. Then, on the basis of the observations made at the end of Section 1, estimated distributions of vehicle speeds are derived from the I-80 dataset (Section 3.2). Bimodal distributions are observed at various occupancy levels, and a new model is proposed to capture those variations (Section 3.3). Possible connections with other theories are then discussed (Section 3.4).

3.1. Microscopic simulation

We study here the variations of the distributions of vehicle speeds as a function of the free-flow speed ϑ and of the occupancy k, using synthetic traffic data sets produced by microscopic traffic simulations on a one-lane ring road. The microscopic model used is the one proposed by [4]. It is able to produce congested traffic states in which the evolution of moving jams induces a bimodal distribution of vehicle speeds.

The free-flow speed, denoted ϑ, varied between $90km.h^{-1}$ and $125km.h^{-1}$. The flow mean occupancy, denoted k, varied between 7.5% and 27.5%. For each pair (ϑ,k), 50 independent micro-simulation runs were recorded. The initial state of each run was homogeneous. Vehicles were evenly distributed on the ring. The length of the ring was set to $L = 1km$. The length of each vehicle was $l = 5m$. The simulated duration of the run was $T = 1h$. The flow mean speed and the interquartile range of the distribution of vehicle speeds are plotted in Figure 5, for $\vartheta = 90km.h^{-1}$ (Figure 5a) and $\vartheta = 125km.h^{-1}$ (Figure 5b), as a function of the flow mean occupancy. In both cases, congested traffic states emerge when the flow mean occupancy exceeds the critical occupancy $k_{c,\vartheta}$. The latter depends on the free-flow speed, and is close to

[4]In Wolfram's CA classification [2].

DOI: 10.1002/atr

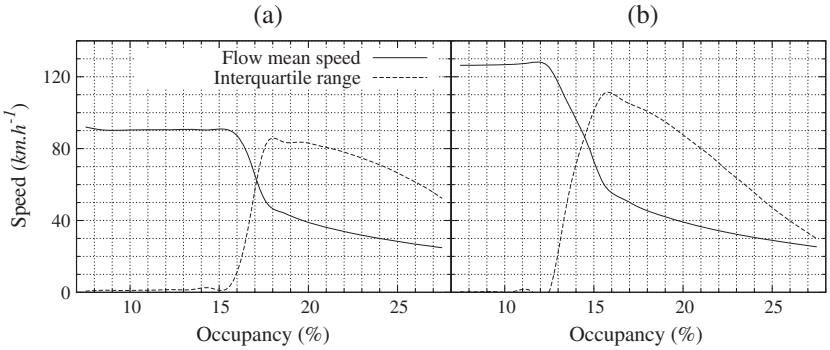

Figure 5. Evolution of the flow mean speed and of the interquartile range of the distribution of vehicle speeds, as a function of the flow mean occupancy. (a) $\vartheta = 90\text{km.h}^{-1}$ and (b) $\vartheta = 125\text{km.h}^{-1}$.

$$k_{c,\vartheta} \approx \frac{1}{1 + \frac{\vartheta \tau_\vartheta}{l}} \tag{1}$$

where τ_ϑ is the inter-vehicle time gap. $k_{c,90} \approx 16\%$ and $k_{c,125} \approx 12.5\%$.

For occupancy less than the critical occupancy, the flow is free. The distribution of vehicle speeds is unimodal, and centered around the free-flow speed. When the occupancy exceeds the critical occupancy, the flow mean speed decreases. The distribution of vehicle speeds becomes bimodal. Moving jammed platoons appear in the flow. The low-speed mode corresponds to vehicles inside a jammed platoon. The high-speed mode corresponds to vehicles evolving outside of a jam. A noticeable fact is that for occupancy values exceeding 17.5%, the average speed are almost equal for both systems, although the high-speed modes of the two distributions are different.

3.2. Estimating the distribution of vehicle speeds

From the fundamental diagram of the I-80 dataset in the occupancy-speed plane (Figure 1), there exists a simple, continuous, one-to-one mapping between the level of congestion (measured by occupancy) and the flow mean speed. Let us denote $\bar{K}(v)$ the relationship between the speed and the occupancy. Let us now assume that a 30-second observed (n,k,v) triple in the I-80 dataset correspond to a platoon of n vehicles observed at the location of loop sensor, with k the 30-second mean occupancy and v the 30-second mean speed. A vehicle in the platoon is indiced by i in $1 \ldots n$. l_i is the length of vehicle i, v_i the speed of vehicle i at the time it crossed the loop, and h_i the time headway, that is, the amount of time that elapsed between the instant when vehicle i-1 did exit the loop and the instant when vehicle i did enter the loop. Let us also assume that $v_i = v + \omega$ with ω a zero-mean low variance Gaussian noise. This hypothesis is supported by the observations made on the RAI distribution of speeds (end of Section 2.4) and origin-of-time invariance arguments.

Under this hypothesis, the distribution of vehicular speeds, denoted as f_v, can be estimated by a Gaussian kernel density estimate

$$f_v \approx \frac{\sum_{(n,v)\in R} \mathcal{N}\left(nv, \sigma^2\right)}{\sum_{(n,v)\in R} n} \tag{2}$$

with $R = \{(n,v)\}$ a set of volume-speed 30-second data records.

If $\overline{K}$ was true at the microscopic level of each vehicle—let us denote this hypothesis the *smooth homogeneous microscopic dynamics hypothesis*—then the vehicular occupancy $k_i = \frac{l_i/v_i}{h_i + l_i/v_i}$ would be such that $k_i = \overline{K}(v) + \varepsilon$ with ε a zero-mean low variance Gaussian noise: vehicles in the platoon could be supposed evenly spaced. One could write

DOI: 10.1002/atr

$$f_v = f_k \circ \overline{K} \tag{3}$$

with f_k estimated by

$$f_k \approx \frac{\sum_{(n,k)\in R} \mathcal{N}\left(nk, \sigma^2\right)}{\sum_{(n,k)\in R} n}$$

and $R = \{(n,k)\}$ a set of volume-occupancy 30-second data records.

If the smooth homogeneous microscopic dynamics hypothesis holds, then the vehicular speed distributions obtained from Equation (3) should be very close to the one from Equation (2). This is not the case for the I-80 dataset. The distribution of vehicular speeds estimated from Equation (2) for lanes 2 to 5 (Figure 6b) shows two distinct peaks—one at $47 km.h^{-1}$, the other at $100 km.h^{-1}$—whereas the distribution of speeds estimated using Equation (3) is a single-peak distribution with a maximum around $95 km.h^{-1}$.

One may argue that, because multiple lanes are observed, this two-peak, bimodal distribution simply reflects the fact that different homogeneous flows are observed, with low vehicles on the low-speed lane (lane 5), high-speed vehicles on the high-speed lane (lane 2), and other vehicles on lanes 3 and 4. If this was the case, then such a bimodal speed distribution should not appear on lane 1. But it does. The two peaks are even sharper on the HOV lane (lane 1) than on the average of all other lanes (Figure 6). Although not plotted here, almost identical plots are obtained for each lane and each detector station. The most frequently observed vehicular occupancy on lane 1 is around 11%. According to the fundamental diagram of lane 1 (Figure 1), this occupancy value corresponds to a flow mean speed of $95 km.h^{-1}$. On average, according to the fundamental diagram, the flow on lane 1 is approaching the criticity threshold but is still in free-flow conditions. Individual vehicle speeds should not vary much. At the same time, the two peaks in the observed estimated distribution of vehicular speeds suggest a complex microscopic dynamics, with vehicle speeds varying in a broad range while driving across the study area.

3.3. Bimodal estimates of vehicle speeds distributions

More remarkably, the bimodal character of the estimated distribution of vehicle speeds remains when analyzing how this distribution varies with occupancy. In Figure 7a (respectively, b and c) is a histogram plot of the estimated distribution of vehicle speeds, for lane 1, for all records such that the occupancy equates 10% (respectively, 13% and 16%). In each case, the histogram is well fitted by summing two distinct distributions. One, the high-speed mode, has a narrow interdecile range and a high-median value. For lane 1, the median of the high-speed mode is close to the speed limit, around $100 km.h^{-1}$. The interdecile range is about $20 km.h^{-1}$-wide around the median. The second

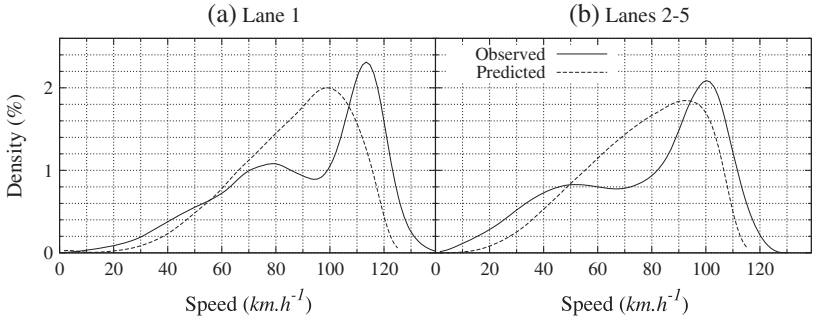

Figure 6. Comparison of vehicular speed distributions estimated from 30-second data. (a) for lane 1 and (b) for lanes 2 to 5. The observed distribution comes from Equation (2). The predicted distribution comes from Equation (3), under the smooth homogeneous microscopic dynamics hypothesis.

DOI: 10.1002/atr

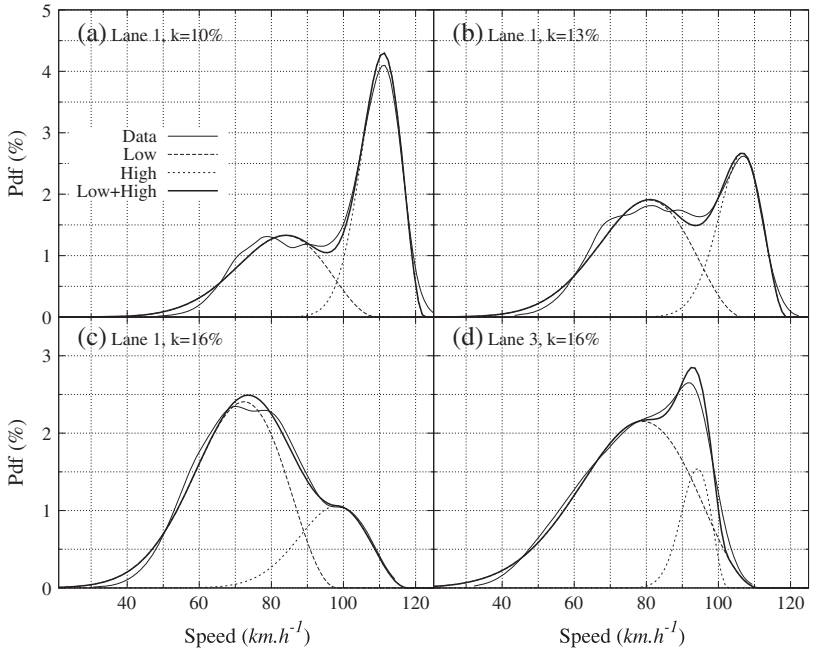

Figure 7. Bimodal estimates of the distribution of vehicle speeds.

distribution, the low-speed mode, has a lower median value and spreads over a larger range than the high-speed mode. For lane 1, the median of the low-speed mode remains around $75km.h^{-1}$ when the occupancy varies between 10% and 16%. It then drops to 45% when the occupancy reaches 20%. The speed values in the low-speed mode spread in a $60km.h^{-1}$-wide interdecile. Similar bimodal distributions, and similar variations of those distributions with occupancy, are observed for all other lanes. See for instance the bimodal estimates of speed distributions for lane 3 and an occupancy of 16% (Figure 7d).

The estimated vehicle speeds distribution plotted in Figure 7 have been fitted[5] with the following model:

$$f_v = \lambda \mathcal{M}_{\check{a},\check{b}} + (1-\lambda)\mathcal{M}_{\hat{a},\hat{b}} \tag{4}$$

with

- $\lambda(k)$ the fraction of vehicles in the low-speed mode, varying continuously from 0 to 1 when the occupancy k varies from 0 to 1.
- $\mathcal{M}_{a,b}$ a Maxwell–Boltzmann-like distribution with a shape parameter a and originated at b, that is

$$\mathcal{M}_{a,b}(v) = \begin{cases} 0 & \text{if } b < v \\ \sqrt{\dfrac{2}{\pi}}\,\dfrac{(b-v)^2}{a^3} e^{-\frac{(b-v)^2}{2a^2}} & \text{otherwise} \end{cases}$$

- $\check{a}(k)$ (respectively, $\hat{a}(k)$) the shape parameter of the low (respectively, high) mode.
- $\check{b}(k)$ (respectively, $\hat{b}(k)$) the maximum speed in the low (respectively, high) mode.

The fitted parameters are given in Table I. In each case, the root-mean square of residuals is quite low. The model explains well the observations.

[5]The fits were computed using the Gnuplot implementation of the nonlinear least-squares Marquardt–Levenberg algorithm.

DOI: 10.1002/atr

Table I. Fitted values of the model's parameters.

Lane, k	λ	$\check{a}$	$\check{b}$	$\hat{a}$	$\hat{b}$	Root-mean square residuals
Lane 1, 10%	0.59	18.0	109	8.09	122	1.7×10^{-3}
Lane 1, 13%	0.40	18.6	107	8.72	119	1.6×10^{-3}
Lane 1, 16%	0.25	18.2	98	14.0	117	1.4×10^{-3}
Lane 3, 16%	0.16	23.0	111	6.0	103	1.3×10^{-3}

3.4. Discussion

The wide scattering of traffic flow data (Figure 3) has been the subject of active research. Macroscopic models derived from the fundamental diagram cannot explain those experimental facts. A number of alternative theories have been proposed, mainly by physicists (see [5] for a detailed review). Among them, one can find the kinetic theory of traffic, Kerner's three-phase flow theory, and the cusp [6] catastrophe model.

The kinetic theory of traffic finds its roots in the works of [7]. They developed a two-fluid model for town traffic [8,9]. One fluid consists of moving vehicles. The other vehicles are stopped as a result of traffic conditions (congestion, traffic signs, etc.). One key parameter is the distribution of desired speeds. Below some critical concentration, the equilibrium distribution of speeds is a one-parameter family. Above that concentration, this flow persists. But another component appears, in which a density-dependent fraction of the traffic is stopped, the remainder being at desired speed. This model has often been criticized in that its derivation into a macroscopic univariate traffic flow model implies the distribution of desired speeds to be non-zero for vanishing speeds. Nelson and Sopasakis have shown that no one-parameter macroscopic model can be derived if this assumption is relaxed, and concluded that two-parameter macroscopic models should be used to describe data scattering [10]. Kerner's theory proposes to classify traffic states into three different phases [11]. One denoted F is free. The two others (S and J) are congested. In the free phase F, the flow increases linearly with the density, up to a metastable region where free phases can coexist with synchronized states in phase S. In the synchronized phase, flow and density are independent of each other. The jammed phase J contains traffic states characterized by a high density and small flow rate/flow speed values. Transitions are allowed between F and S, and between S and J, but not between F and J. Navin suggested the three-dimensional cusp catastrophe to be appropriate for traffic variables [12]. The surface of the cusp catastrophe is defined by two control variables with smooth continuous changes, whereas the state variable is subject to discontinuities. Navin suggested using the flow rate and the occupancy as control variables, and speed as state variable. Hall has conducted further studies in this line of ideas [13].

The three theories sketched previously express the same general idea. There is an occupancy region, between free flow and jammed flow, where no univariate macroscopic flow model applies. But they seem to lack a unifying framework. The model expressed by Equation (4) seems promising to this end. To the best of the author's knowledge, it is the first macroscopic model that links explicitly the occupancy with the distribution of vehicular speeds in the flow of traffic. As such, and being enthusiastic, it can be seen as a new kind of fundamental diagram, the mean flow speed being replaced by a random variable with a well-defined probability density function. A lot of work remains to be performed to assess the validity of this statement. Bias may exist in the I-80 dataset. Other datasets should be analyzed to confirm the validity of the model. Some avenues of exploration are drawn in the conclusion of this paper.

4. APPLICATION TO FUEL CONSUMPTION MODELING

The purpose of this section is to design a simple and naïve FC model called BIMODACT (for BIMODal ACTivity), to compute link-based FC from link-based traffic data. We concentrate here on FC because it is the primary determinant for other out-of-pipe emissions. BIMODACT is simple

[6] In Thom's catastrophe theory terminology [6].

DOI: 10.1002/atr

in that it relies on simple models: (i) a trip-average speed FC model; and (ii) on bimodal speed distributions to capture the impact of speed variability on emissions. It is naïve in that a large part of what makes the complexity of operational traffic emission models is omitted. This section is organized as follows. Section 4.1 gives some of our motivations for this work. Two FC models are presented in Section 4.2. One, taken from COPERT 4, is used to compose BIMODACT. The other, called Comprehensive Modal Emission Model (CMEM), is used as a yardstick. BIMODACT is defined in Section 4.3, and applied on real world data in Section 4.4.

4.1. Motivations

There is a mismatch between the traffic activity data required by mobile sources emission models and today's available traffic data. On the one hand, emission models use trip-based data, such as trip length and trip average speed. On the other hand, traffic sensors do measure traffic flow variables at point-based locations on road links. At the same time, the need for air quality assessments of traffic demand management policies is increasing. To this end, mobile sources emission models provide the necessary inputs to photochemical models, with a typical $1h/1km$ time/space resolution for metropolitan area. Those requirements have led to the development of a new generation of mobile sources emission models—exemplified by the US Environmental Protection Agency's MOtor Vehicle Emission Simulator (MOVES) model—for which the necessary traffic activity data is recommended to be derived from a travel demand model. To illustrate the complexity of the needed data, the following sentences are quoted from MOVES documentation: *Vehicle power, speed, and acceleration have a significant effect on vehicle emissions. At the County scale, MOVES models those emission effects by using distribution of vehicles hour traveled (VHT) by average speed. MOVES in turn uses the average speed distribution to select specific drive cycles, and MOVES uses these drive cycles to calculate operating mode distributions. The operating mode distributions in turn determine the calculated emissions rates. … A local speed distribution by road type and source type is necessary. MOVES calls for a speed distribution in 16 speed bins, by each road type, source type, and hour of the day included in the analysis*. If the available drive cycles do not cover all the possible (road-type, source type, and average speed) combinations, one has to use microscopic traffic simulator to this end. But even state-of-the-art microscopic models, such as AIMSUN and VISSIM, have been reported to fail in producing realistic enough vehicle trajectories with respect to emission modeling [14,15]. Also, using a travel demand model to estimate route flows for the purpose of emission modeling, as suggested for MOVES, is highly questionable. The stability of route flow (and even link flow) solutions in dynamic multiclass user-equilibrium traffic assignment is still a research topic [16,17]. Possibly drastically different route flow equilibria, hence emission patterns, may be computed for a given demand. The authors are not aware of good practices to evaluate the stability of solutions resulting from dynamic traffic assignment tools, not accounting for calibration issues [18]. Last, but not the least, the day-to-day variability in traffic demand and traffic patterns has to be dealt with in an appropriate manner when bridging together an emission model and a photochemical model. For instance, it has been shown in Section 2 how the distribution of average speeds during the evening peak period of the I-80 dataset varies. Ensemble techniques like those used in probabilistic weather prediction may help in dealing with all those sources of uncertainties, at the price of a huge increase in computational requirements. Hundreds of traffic simulation/emission estimates, with random perturbations of the inputs, would be required. All this foreseen complexity pleads for direct methods to compute link-based traffic emissions from link-based traffic data.

4.2. Fuel consumption modeling

Fuel consumption models are a core component of road traffic emission models. Many emission models have been proposed in the literature (see for instance [19] and references therein). Most of them are trip-based and specify—or can be used to specify—*emission factors* usually expressed in $g.km^{-1}$. Emission factors are defined for classes of vehicles rather than for every model available on the market. To this end, vehicles are categorized into classes according to a number of characteristics, including the vehicle type (e.g., two wheels, passenger cars, and heavy or light duty), the fuel used (e.g., gasoline, diesel, and natural gas), the weight, the engine size, and the

DOI: 10.1002/atr

regulated emission standard. Depending on the level of detail available for a given trip, different emission models can apply. On one side of the spectrum, *average-speed models* (such as COPERT 4, EMFAC or MOBILE 6) express emission factors as a function of the mean trip speed. By definition, an average-speed model cannot distinguish between trips with the same mean speed but different speed profiles. On the other side of the spectrum, *physical power demand models*, also called *instantaneous models*, do compute second-by-second tail pipe emissions on the basis of (i) a detailed description of the vehicle's subsystems (e.g., engine, power-train, and auxiliaries); and (ii) the second-by-second vehicle's operating conditions (speed, acceleration, and road grade). Besides vehicle classes and trip data, other inputs are required. Indeed, vehicle emissions depend on several other factors, including the road gradient, the vehicle load, the weather conditions, and the age of the vehicle. Also, the literature distinguishes between evaporative emissions, cold start emissions, and hot emissions. But despite their differences, most emission models do rely on a core FC model under hot stabilized engine conditions. In what follows, the two following FC models are considered. The first is an average-speed model taken from COPERT 4. The second comes from CMEM. Both are described and compared hereafter.

4.2.1. COPERT

The COPERT 4 methodology, included in the EMEP/EEA emission inventory guidebook [20], is widely used in Europe. It is based upon average-speed emission factors. For a given class of vehicles, the mass E_p of a pollutant p emitted during a trip of length L and of duration T is given by $E_p = Le_p(\overline{v})$, where $\overline{v} = L/T$ is the trip-average speed, and e_p is the emission factor for the pollutant p.

As an example, the COPERT 4 emission factors for *Euro 1 and later gasoline passenger cars* and p in $\{CO, HC, NO_x\}$ are of the form

$$e_p(\overline{v}) = \frac{a_1 + a_2\overline{v} + a_3\overline{v}^2}{1 + a_4\overline{v} + a_5\overline{v}^2} \tag{5}$$

with $\overline{v}$ in the range $[10:130]km.h^{-1}$. The FC is also predicted using Equation (5). Note that Equation (5) does not stand for all vehicle classes, or for all pollutants. For instance, the emission factor for CO_2 is a linear combination of FC and other emission factors. Generally speaking, COPERT emission factors are nonlinear U-shape functions (Figure 8a).

4.2.2. Comprehensive Modal Emission Model

The Comprehensive Modal Emission Model (CMEM) is a modal emission model. It is public-domain and maintained by the Center for Environmental Research and Technology, University of California, Riverside. CMEM is based on six physical sub-models that predict engine power, engine speed,

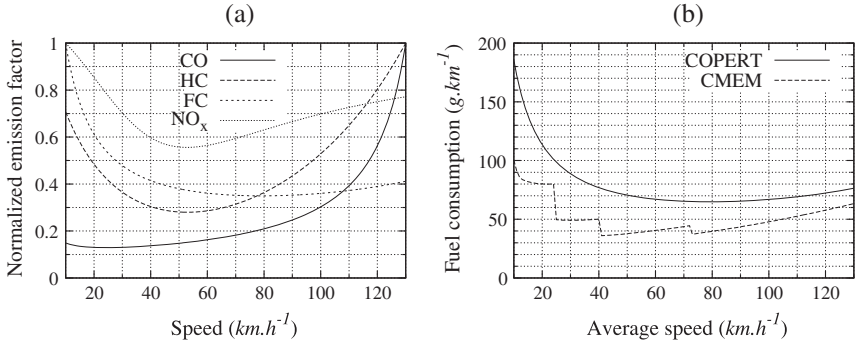

Figure 8. (a) Normalized COPERT emission factors for CO, HC, and NO_x and the fuel consumption FC, for EURO 2 gasoline passenger cars. (b) Comparison of the fuel consumption predicted by COPERT and CMEM for the *gasoline passenger car*, using constant speed profiles.

DOI: 10.1002/atr

air-to-fuel ratio, FC, engine-out emissions, and catalyst pass fraction, depending on vehicle's operation variables (e.g., speed, acceleration, and road grade). According to CMEM's documentation the instantaneous FC, expressed in $g.s^{-1}$ and denoted hereafter $FC(t)$, is computed by

$$FC(t) = \begin{cases} \phi(t)\cdot\left(K(t)\cdot N(t)\cdot V + \dfrac{P(t)}{\eta}\right)\cdot\dfrac{1}{LHV} & \text{for } P > 0 \\ K_0 N_0 V & \text{for } P = 0, \end{cases}$$

where $\phi(t)$ is the air-to-fuel ratio, $P(t)$ is the engine power output, $K(t)$ is the engine friction factor, $N(t)$ is the engine speed (in revolutions per second), V is the engine displacement, η is a measure of indicated efficiency, and LHV the lower heating value of the fuel used. K_0 (respectively, N_0) is the engine friction factor (respectively, engine speed) during engine idling. Hot-stabilized engine-out emission rates are then computed by multiplying FC by pollutant specific engine-out emission index. The minimal trip input data required by CMEM are a speed profile (i.e., a list of time-stamped speed values), with a typical sampling frequency of 1 Hz (although this is not a requirement).

4.2.3. COPERT compared with CMEM

COPERT and CMEM have been developed in countries having noticeably different vehicle fleets and emission regulations. Hence, there is no obvious mapping between the way vehicles have been categorized in both models. Anyway, the CMEM vehicle class *gasoline Tier 1*, *mileage* $< 50k$, *low power/weight*, and the COPERT 4 vehicle class *EURO 2 gasoline passenger car*, *engine capacity* $\geq 2l$ present very similar characteristics. In what follows, this particular vehicle class is denoted as *gasoline passenger car*.

We compared the FC predicted by COPERT 4 and CMEM for the gasoline passenger car, as a function of the trip average speed. We first applied CMEM on speed profiles simulating trips traveled at constant speed, for speeds in the range $[10;130] km.h^{-1}$. The FC rates predicted by CMEM for those constant speed profiles, expressed in $g.km^{-1}$, are far below the one predicted by COPERT 4 (Figure 8b). The relative difference is close to 80% at $10 km.h^{-1}$. It then decreases when the speed increases. At $130 km.h^{-1}$, the relative difference is around 20%. This comes with no surprise. As an average speed model, the COPERT 4 FC model implicitly assumes trips with several acceleration, cruise, and deceleration phases.

When fed with more realistic inputs, CMEM and COPERT do better match. The Common ARTEMIS Driving Cycles (CADC) has been developed within the European project ARTEMIS (Assessment and Reliability of Transport Emission Models and Inventory Systems). They have been designed to be statistically representative of real world driving patterns. The CADC include the two following driving

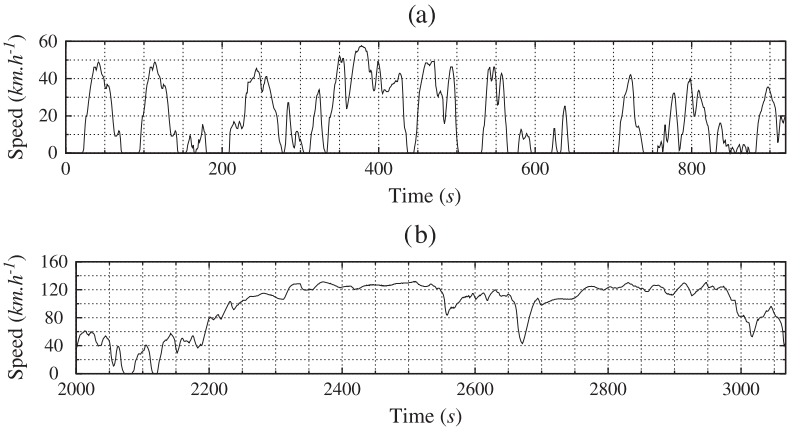

Figure 9. Artemis driving cycles. (a) Artemis Urban Cycle. (b) Artemis Motorway130 Cycle.

DOI: 10.1002/atr

Table II. Fuel consumption predicted by the Comprehensive Modal Emission Model and COPERT for the gasoline passenger car for the *Urban* and *Motorway130* ARTEMIS driving cycles.

Driving cycle	Comprehensive Modal Emission Model	COPERT	Relative difference
Urban	113.96 $g.km^{-1}$	123.5 $g.km^{-1}$	7.7%
Motorway130	62.20 $g.km^{-1}$	66.31 $g.km^{-1}$	6.2%

cycles: *Urban* and *Motorway130*. The speed profiles of those cycles are plotted in Figure 9. Their detailed characteristics can be found in [21]. The *Urban* cycle has an average speed of 17.5$km.h^{-1}$ and a running speed of 24.4$km.h^{-1}$ (the vehicle is at full stop during 28% of the cycle duration, for a total of 21 stops). The *Motorway130* cycle contains no stop. Its average speed is of 116$km.h^{-1}$. The FC predicted by CMEM and COPERT for the *gasoline passenger car* on the *Urban* and *Motorway130* driving cycles are given in Table II. The relative difference is 6.2% (respectively, 7.7%) for the *Motorway130* (respectively, *Urban*) driving cycle.

Having no information on (i) the error margins of each models; and (ii) the differences between the vehicle classes chosen in both models for the *gasoline passenger car*, we now assume that both models are properly calibrated. CMEM will be used as a yardstick when vehicle trajectory data are available.

4.3. Bimodal fuel consumption modeling

Let us consider the situation, similar to the one simulated in Section 3.1, where $n = k_l^L$ identical vehicles of length l are distributed on a ring road of length L, with a mean-occupancy k and a free-flow speed set to ϑ. The purpose is to estimate the quantity C of fuel consumed during a time interval of duration T, as a function of k and ϑ. We have at our disposal an instantaneous FC model denoted as c (e.g., CMEM) and an average speed FC model $\overline{c}$ (e.g., COPERT). v_i denotes the speed profile of vehicle i. T is taken long enough so that the system can be supposed ergodic; that is, spatial and temporal distributions of vehicle speeds are assumed identical. In other words, if one had observed the probability density function f of vehicle speeds at a particular point of the ring during the period T, then for any vehicle i, any instant t, and any interval $[a,b]$ the following holds:

$$Pr(a < v_i(t) < b) = \int_a^b f(v)\ \mathrm{d}v$$

Under this hypothesis, the trip average speed $\overline{v}_i$ of any vehicle i equates the flow mean speed $\overline{v}$, that is:

$$\overline{v}_i = \frac{1}{T}\int_0^T v_i(t)\ \mathrm{d}t = \int v f(v)\ \mathrm{d}v = \overline{v} \tag{6}$$

C can be expressed in three ways. First, using the average speed FC model $\overline{c}$ and summing over trips using Equation (6), we have

$$C_1 = \sum_{i=1\ldots n} \overline{c}(\overline{v}_i)\int_0^T v_i(t)\ \mathrm{d}t = k\frac{L}{l}\overline{v}T\cdot\overline{c}(\overline{v}) \tag{7}$$

Second, using the vehicles' speed profiles and the instantaneous FC model c, we have

$$C_2 = \sum_{i=1\ldots n} c(v_i) \tag{8}$$

DOI: 10.1002/atr

Third, using the average speed FC model and the probability density function of flow speed,

$$C = k\frac{L}{l}\overline{v}T\int f(v)\overline{c}(v)\ \mathrm{d}v$$

Results from Section 3 suggest that the probability density function of vehicle speeds f can be approximated by a bimodal distribution, using a probability density function of the form $f = \lambda_k f_{k,v} + (1-\lambda_k)f_{k,\hat{v}}$. Let us now assume that

$$\begin{aligned} f &= \lambda\delta_{\underline{v}} + (1-\lambda)\delta_{\vartheta} \\ \lambda &= min\left(1, max\left(0, \frac{\vartheta - \overline{v}}{\overline{v} - \underline{v}}\right)\right) \end{aligned}$$

That is (i) the high-speed mode $f_{k,\hat{v}}$ is now supposed not to vary with k and is reduced to a Dirac delta located at the free-flow speed ϑ; (ii) the low-speed mode $f_{k,v}$ is now supposed not to vary with k and is reduced to a Dirac delta located at a constant low speed $\underline{v}$. The Dirac delta account for the fact that speed distributions are implicitly assumed by the average speed model, in that an average speed is representative of a driving cycle. The low (respectively, high) is supposedly constant to make things as simpler as they can be. We now have

$$\begin{aligned} C_3 &= k\frac{L}{l}\overline{v}T\left(\lambda\overline{c}\left(\underline{v}\right) + (1-\lambda)\overline{c}(\vartheta)\right) \\ \lambda &= min\left(1, max\left(0, \frac{\vartheta - \overline{v}}{\overline{v} - \underline{v}}\right)\right) \end{aligned} \tag{9}$$

Equation (9) defines BIMODACT. It basically depends on two, road dependant parameters: the free-flow speed ϑ and the low speed $\underline{v}$. The FC estimates using COPERT (Equation (7)), CMEM (Equation (8)) and BIMODACT (Equation (9)) have been computed using the same set of simulation runs than those described in Section 3.1. The results are plotted in Figure 10, for $\vartheta = 90km.h^{-1}$ and $\vartheta = 125km.h^{-1}$. In both cases, $\underline{v}$ was set to $20km.h^{-1}$. When the occupancy is below the critical occupancy, BIMODACT equates COPERT. In this case, the flow-mean speed $\overline{v}$ equates the free-flow speed ϑ. Hence, $\lambda = 0$ in Equation (9), which becomes Equation (7). CMEM is below COPERT, for the similar reasons than those exposed in Section 4.2.3. Differences appear when the occupancy exceeds the critical occupancy. In congested traffic states, BIMODACT is higher than COPERT, and noticeably close to CMEM. The difference between BIMODACT and COPERT increases as soon as congestion appears.

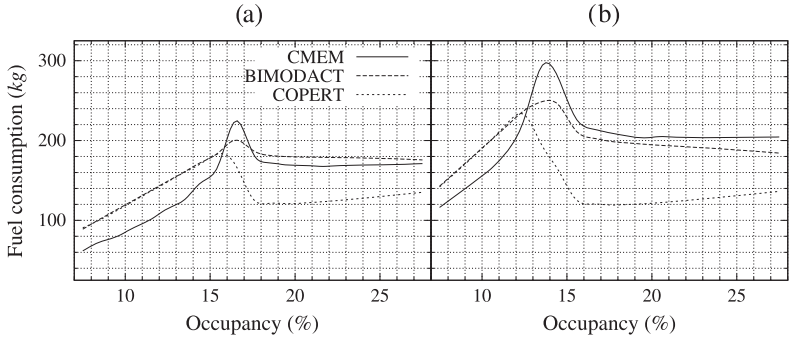

Figure 10. Fuel consumed during 1 hour for the simulated data, as a function of the flow occupancy.

DOI: 10.1002/atr

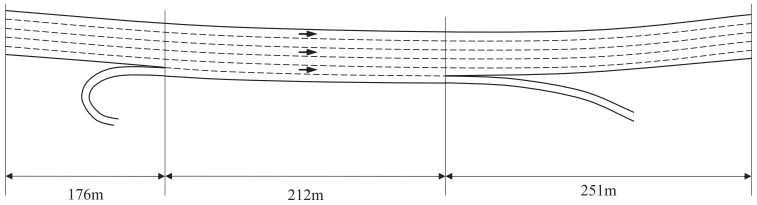

Figure 11. Schematic top view of the freeway segment of US 101 (Hollywood Freeway, Los Angeles, California) on which the trajectory data have been collected.

4.4. Experiments on real data

The results presented in Section 4.3 show that, in simulated congested conditions, BIMODACT allows for FC estimates that are close to those produced by CMEM. However, the set of simulated vehicle trajectories that has been used may introduce some bias. First, the simulated data were intentionally built so that the distribution of vehicle speeds is ergodic. Second, the dynamics of vehicle trajectories produced by the microscopic traffic model does not reflect all aspects of real-world vehicle trajectories.

In this section, COPERT, CMEM, and BIMODACT are tested using real trajectory data from the American project NGSIM [22]. First, the dataset is described in Section 4.4.1. Then in Section 4.4.2, the three models are applied on vehicle trajectories. Finally in Section 4.4.3, COPERT and BIMODACT are applied using traffic detector data.

4.4.1. Description of the data

The US101 NGSIM dataset has been collected on the southbound direction of Hollywood Freeway, a freeway segment of US Highway 101 in Los Angeles, California. Figure 11 provides a schematic top view of this road segment. The site is approximately 640m in length, with five main lanes and one auxiliary lane throughout the section. Lanes are numbered from 1 to 6, starting from the left-most lane to the auxiliary lane. The speed limit is 65mph, which is close to 104$km.h^{-1}$. Vehicle trajectories were measured using video cameras, and sampled at a resolution of 10 frames per second, between 7:50 and 8:35 AM. A total of 6101 trajectories, among which 45 are motorcycles trajectories and 137 are long vehicles (i.e., trucks and buses) trajectories, are available. In what follows, motorcycles and long vehicles are not considered. The trajectories observed on lane 1 are plotted in the time-space diagram, as shown in Figure 12. One can clearly see traffic waves moving in the opposite direction of the traffic flow. The traffic is in a congested state. The passenger car average speed over the section is 33.2$km.h^{-1}$, with a standard deviation equal to 15.6$km.h^{-1}$.

4.4.2. Fuel consumption using vehicles trajectories

The total FC is estimated for the passenger car trajectories contained in the US101 NGSIM dataset, using the same three methods than those exposed in Section 4.2.3. It is assumed that all vehicles belong to the gasoline passenger car class. Using Equation (7) (i.e., COPERT), we found out that

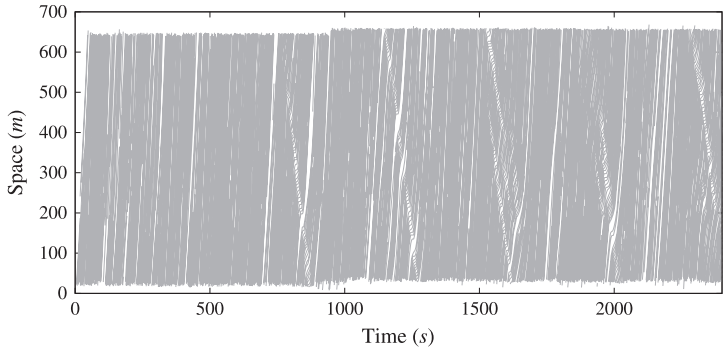

Figure 12. Vehicles trajectories observed on lane 1 of the US101 NGSIM dataset.

DOI: 10.1002/atr

the total FC amounts to $303kg$. Using Equation (8) (i.e., CMEM), we found out that it amounts to $384kg$. As observed with the simulated congested data, COPERT underestimates the value obtained with CMEM. A difference of approximately 21% is observed for the NGSIM trajectories. Using Equation (9) (i.e., BIMODACT), with $\vartheta = 104km.h^{-1}$ and $\underline{v} = 20km.h^{-1}$, we get $376kg$, a 2% relative difference with CMEM.

Besides differences in the total FC, the use of individual vehicle trajectories allows for a closer examination of where the models diverge. For a given trajectory (i.e., speed profile) v_i, let us denote $r(v_i)$ the speed interquartile range of vehicle i. $r(v_i)$ follows the standard definition it was given in the field of descriptive statistics. It is the difference between the third and the first quartile of the distribution of values in v_i. To compare CMEM and COPERT, we computed the following mean differences:

$$\Delta_k = \frac{1}{\#C_k} \sum_{i \in C_k} (e_m(v_i) - l_i e_M(\overline{v}_i))$$

where $C_k = \{i, r(v_i) \in b_k\}$ is the set of vehicles having their speed interquartile range in the interval $b_k = [\mathrm{k}\Delta\mathrm{v}, (k+1)\Delta\mathrm{v})$, $k = 0, 1, \ldots$, and $\Delta\mathrm{v}$ is set to $2.5km.h^{-1}$. The same quantities were computed for CMEM and BIMODACT.

Results are plotted in Figure 13. The mean difference between CMEM and COPERT increases when the speed interquartile range increases from 0 to $10km.h^{-1}$. It then remains almost constant, around $12g$ (to be compared with the mean FC per trajectory predicted by CMEM, around $66g$). This observation confirms that COPERT intrinsically underestimates the emissions for congested traffic states, when compared with CMEM. *A contrario*, BIMODACT estimates are very close to CMEM's.

4.4.3. Estimation of the fuel consumption using traffic detector data

The US101 NGSIM dataset contains the 5-minute average speed and the 5-minute average occupancy measured by a loop sensor. Here we make use of those data to estimate the FC predicted by COPERT and BIMODACT. Using COPERT, we found out that the total FC is given by:

$$5L \sum_j \overline{q}_j \cdot e_M(\overline{v}_j)$$

where $L = 640m$ is the length of the road segment, j is the index of a 5-minute interval in [7:50,8:35], $\overline{q}_j$ (in $veh.h^{-1}$) is the 5-minute mean flow rate, and $\overline{v}_j$ (in $km.h^{-1}$) is the 5-minute mean flow speed. It

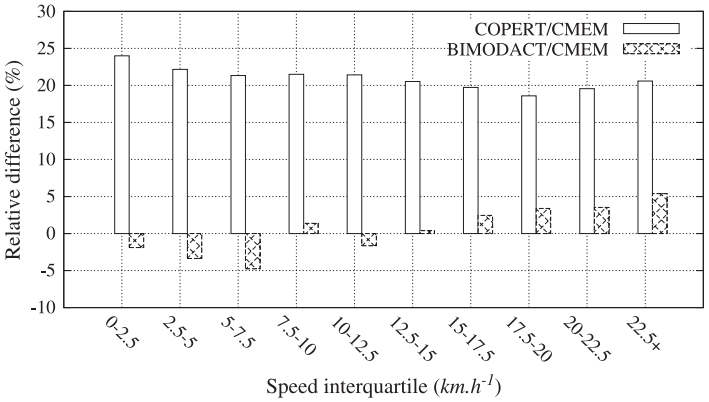

Figure 13. Fuel consumption using vehicle trajectories.

DOI: 10.1002/atr

amounts to $316kg$, to be compared with $384kg$ obtained with CMEM and trajectory data. Using BIMODACT, we found out that the total FC is given by:

$$5L\sum_j \overline{q}_j\left(\lambda_j e_M\left(\underline{v}\right) + \left(1-\lambda_j\right)e_M(\vartheta)\right)$$

with $\lambda_j = min\left(1, max\left(0, \frac{\vartheta-\overline{v}_j}{\overline{v}_{j-}\underline{v}}\right)\right)$, $\vartheta = 104km.h^{-1}$, and $\underline{v} = 20km.h^{-1}$. It amounts to $394kg$, to be compared with $384kg$ obtained with CMEM and trajectory data.

5. CONCLUSION

The main contribution of this paper is the model defined in Section 3.3. It expresses the distribution of vehicle speeds in traffic flow f_v as a function of the occupancy k, with five parameters.

$$f_v = \lambda\mathcal{M}_{\check{a},\check{b}} + (1-\lambda)\mathcal{M}_{\hat{a},\hat{b}}$$

with $\mathcal{M}_{a,b}$ a Maxwell–Boltzmann distribution, $\check{a}$ (respectively, $\hat{a}$) the shape parameter of the low (respectively, high) mode, $\check{b}$ (respectively, $\hat{b}$) the maximum speed in the low (respectively, high) mode, and a the fraction of vehicles in the low mode. The model is not yet fully specified. We do not propose here a functional form (as a function of occupancy) for the parameters. This is left to the near future, along with complementary studies of empirical traffic data.

This model has strong connections with the kinetic theory of traffic flow, where the unknown is precisely a distribution of vehicle speeds, as a function of space and time. We plan to investigate this point. Numerical and/or analytical solutions of kinetic models may be found more easily by constraining the shape of the solutions. We also foresee interesting applications in the validation and calibration of microscopic traffic models, and a better understanding of micro–macro relationships.

On the practical side, a typical application that relies on a statistical description of vehicle operating modes (starting with the speed) is traffic emission modeling. The ability to derive some of the needed traffic activity statistics directly from traffic flow data can help in feeding the new generation of emission models. As an example, a simple FC model, BIMODACT, has been defined. BIMODACT can use standard 5-minute traffic flow data and still produce FC estimates close to the instantaneous emission model CMEM, taken as a yardstick. BIMODACT is essentially parametrized by two values, the free-flow speed ϑ and the low-speed mode $\underline{v}$. Both should be easy to calibrate using existing traffic data. With respect to state-of-the-art practice in road traffic emission modeling, BIMODACT is rather crude: traffic activity is binned into two speed modes. It would certainly be interesting to study more elaborate ways to disgregate the new kind of fundamental diagram we propose in this paper into the vehicle-specific power bins required by the current generation of road traffic emission models.

6. LIST OF SYMBOLS

Symbol	Term	Definition
$Pr(a \leq X \leq b)$	Probability	Probability that the random variable X takes a value in the range $[a : b]$
fx	Probability density function (pdf)	If the random variable X has a density, fx denotes the probability density function of the random variable X
$\mathcal{N}(m, \sigma^2)$		Pdf of a normally distributed random variable (or Gaussian variable) with mean m and variance σ^2
δ_m	Dirac delta	The Dirac delta function centered at m, i.e. the limit (in the sense of

(*Continues*)

DOI: 10.1002/atr

Symbol	Term	Definition
		distributions) of a sequence $\mathcal{N}(m, \sigma^2)$ as $\sigma \to 0$
$\mathcal{M}_{a,b}$	Maxwell-Boltzmann pdf	Pdf of a Maxwell-Boltzmann, originated at b, with a shape parameter a. Formally, for $x > b$, $\mathcal{M}_{a,b}(x) = \sqrt{\frac{2}{\pi}} \frac{(b-x)^2}{a^3} e^{-\frac{(b-x)^2}{2a^2}}$
v_i	Vehicular speed	Speed of a given vehicle, indiced by i. $v_i(t)$ if the vehicular speed as a function of time; $v_i(x)$ the vehicular speed as a function of space.
$\overline{v}$ (or simply v)	Flow mean speed	Time mean speed of the flow of vehicles, observed at a particular point of the road during a lapse of time.
k	Occupancy	Point based occupancy, defined as the percentage of time that a particular point of the road is occupied by a vehicle during a lapse of time.
ϑ	Free flow speed	The expected flow mean speed when the occupancy tends towards 0.

ACKNOWLEDGEMENTS

The authors acknowledge the support from VINCI / ParisTech Grant 8L1142 entitled "Éco-Conception des ensembles bâtis et des infrastructures".

Thanks are due to the reviewers of earlier versions of this paper for their fruitful comments.

REFERENCES

1. Greenshields Symp. *75 Years of the Fundamental Diagram for Traffic Flow Theory - Proceedings of the Greenshields Symposium*, number E-C149, 2011.
2. Wolfram S. *A new Kind of Science*. Wolfram Media: Champaign, Illinois, USA, 2002.
3. Maerivoet S, De Moor B. Cellular automata models of road traffic. *Physics Reports* 2005; **419**(1):1–64.
4. Tordeux A, Roussignol M, Lassarre S. An adaptive time gap car-following model. *Transportation Research Part B* 2010; **44**(8-9):1115–1131.
5. Chowdhury D, Santen L, Schadschneider A. Statistical physics of vehicular traffic and some related systems. *Physics Reports* 2000; **329**(4-6):199–329.
6. Thom R. *Structural Stability and Morphogenesis: An Outline of a General Theory of Models*. Addison-Wesley: Reading, Massachusets, USA, 1989.
7. Prigogine I, Herman R. *Kinetic Theory of Vehicular Traffic*. American Elsevier Pub. Co.: New York, 1971.
8. Herman R, Lam T, Prigogine I. Kinetic theory of vehicular traffic: comparison with data. *Transportation Science* 1972; **6**:440–452.
9. Herman R, Prigogine I. A two-fluid approach to town traffic. *Science* 1979; **204**(4389):148–151.
10. Nelson P, Sopasakis A. The Prigogine–Herman kinetic model predicts widely scattered traffic flow data at high concentrations. *Transportation Research Part B: Methodological* 1998; **320**(8):589–604.
11. Kerner B. *The Physics of Traffic*. Springer-Verlag: Berlin, 2004. ISBN: 978-3-642-02604-1.
12. Navin F. Traffic congestion catastrophes. *Transportation Planning Technology* 1986; **11**:19–25.
13. Hall FL. An interpretation of speed-flow-concentration relationships using catastrophe theory. *Transportation Research Part A* 1987; **21**(3):191–201.
14. Smit R, Pae H, McBroom J. Technical note: use of microscopic simulation models to predict traffic emissions. *Road and Transport Research Journal* 2009; **18**(2):49–54.
15. Song G, Yu L, Zhang Y. Applicability of traffic microsimulation models in vehicle emissions estimates: case study of VISSIM. *Transportation Research Record: Journal of the Transportation Research Board* 2012; (2270):132–141.
16. Bliemer M, Bovy CJ, Piet HL. Quasi-variational inequality formulation of the multiclass dynamic traffic assignment problem. *Transportation Research, Part B* 2003; **370**(6):501–519.
17. Lu S, Nie Y. Stability of user-equilibrium route flow solutions for the traffic assignment problem. *Transportation Research Part B* 2010; **44**(4):609–617.
18. Chiu Y-C, Bottom J, Mahut M, *et al*. A primer for dynamic traffic assignment. *Technical report*, ADB30 Transportation Network Modeling Committee - Transportation Research Board, 2010.

DOI: 10.1002/atr

19. Boulter P, McCrae I. Artemis: Assessment and reliability of transport emission models and inventory systems: TRL final report. *Technical report*, Wokingham, UK, 2007.
20. EEA. EMEP/EEA Air Pollutant Emission Inventory Guidebook, 2009. Available from: http://www.eea.europa.eu/publications/emep-eea-emission-inventory-guidebook-2009.
21. André M. Real-world driving cycles for measuring cars pollutant emissions - part A : the Artemis European driving cycles. INRETS report, Bron, France, nlte 0411. *Technical report*, 2004.
22. FHWA. US Department of Transportation, Federal Highway Administration, Next Generation SIMulation (NGSIM), 2008. Available from: http://ngsim-community.org/.

DOI: 10.1002/atr